Dalton Transactions

Accepted Manuscript

ROYAL SOCIETY OF CHEMISTRY

www.rsc.org/dalton

Temperature-dependent Studies of Niccolite Metal Formate Frameworks $[(CH_3)_2NH_2][Fe^{III}M^{II}(HCOO)_6]$ (M=Fe and Mg): Structural, Magnetic, Dielectric and Phonon Properties

Aneta Ciupa,[a] Mirosław Mączka,*[,a] Anna Gągor, [a] Adam Sieradzki,[b] Justyna Trzmiel,[b] Adam Pikul,[a] and M. Ptak[a]

ABSTRACT

Novel heterometallic formate $[(CH_3)_2NH_2][Fe^{III}Mg^{II}(HCOO)_6]$ (DMFeMg) was prepared and characterized by single crystal X-ray diffraction, DSC, dielectric, magnetic susceptibility, Raman and IR methods. We also report thermal, Raman and IR studies of the known compound $[(CH_3)_2NH_2][Fe^{III}Fe^{II}(HCOO)_6]$ (DMFeFe). DMFeMg crystallizes in the niccolite structure ($P\bar{3}1c$ space group). Contrary to the known DMFeFe, $[(CH_3)_2NH_2][Fe^{III}Mn^{II}(HCOO)_6]$ (DMFeMn) and $[(CH_3)_2NH_2][Fe^{III}Co^{II}(HCOO)_6]$ (DMFeCo) formates, the metal ions in DMFeMg are distributed statistically over the two available octahedral sites. Temperature-dependent studies show that whereas DMFeFe exhibits an order-disorder phase transition at 151.8 K upon cooling, freezing-in of reorientational motions of DMA^+ cations does not lead to any structural phase transition in DMFeMg. We discuss origin of this difference. The low-temperature studies also show that DMFeMg orders magnetically at T_C = 13.5(5) K and the shape of $M(T)$ measured in the field-cooling regime suggests ferromagnetic character of the ordering.

Introduction

Metal-organic frameworks (MOFs) are known to posses various functionalities, which can be tuned by using different organic ligands and metal ions.[1] Among this huge class of MOFs, metal formate frameworks attracted a lot of attention in recent years since the $HCOO^-$ ion is capable of mediating ferro- or antiferromagnetic coupling between metal ions due to its small size.[2] As a result, many metal formate frameworks exhibit interesting magnetic properties.[2] Furthermore, many of these compounds show rich polymorphism and ferroelectricity.[2-4] Metal formate frameworks of general formula $[cat][M(HCOO)_3]$ with M=Mg, Zn, Mn, Ni, Co, Fe, and cat = ammonium, methylammonium, dimethylammonium (DMA) etc., have been particularly extensively studied due to their polymorphism, magnetic and multiferroic properties.[5-11] These compounds are also of interest due to their gas sorption capacity and glassy behavior.[12]

Contrary to extensively studied $[cat][M(HCOO)_3]$ frameworks with M= divalent cation, there are only a few reports on synthesis and properties of heterometallic and mixed-valence formate frameworks. Hagen *et al.* reported in 2009 the metal formate framework containing mixed-valence iron(II)-iron(III) cations, DMFeFe, which is a Néel N-Type ferrimagnet.[13] This compound crystallizes in the niccolite type structure (space group $P\bar{3}1c$) with the disordered DMA^+ cations located in the cages of the network.[13] More recently, the phase transition into antiferroelectric phase (space group $R\bar{3}c$) was found for this compound at about155 K.[14] It was reported that this transition involves ordering of DMA^+ cations.[14] Zhao *et al.* succeeded in synthesis of two heterometallic frameworks, DMFeMn and DMFeCo. The former one is an antiferromagnet and the latter ferrimagnet, respectively.[15] Very recently, we have reported

synthesis and properties of heterometallic metal formate $[(CH_3)_2NH_2][Na_{0.5}Fe_{0.5}(HCOO)_3]$ (DMNaFe), which crystallizes in a perovskite-type structure (space group $R\bar{3}$).[16]

Herein, following our search for novel metal formate frameworks with useful functionalities, we report synthesis as well as structural, thermal, phonon, magnetic and dielectric properties of novel DMFeMg. We also report temperature-dependent studies of the known DMFeFe. We would like to emphasize that room-temperature Raman and temperature-dependent IR studies have not yet been reported for DMFeM niccolites. Dielectric data were reported for DMFeFe by Cañadillas-Delgado but only at 10 kHz,[14] and in the present study we report the temperature dependent of the real and imaginary part of the complex permittivity of DMFeFe and DMFeMg measured at various frequencies. These additional measurements provide deeper insight into mechanism of the structural phase transition observed in DMFeFe.

Experimental

Materials and instrumentation

All reagents (analytically grade) used for synthesis are commercially available and used without further purification. Heat capacity was measured using Mettler Toledo DSC-1 calorimeter with high resolution of 0.4 μW. Nitrogen was used as a purging gas. Weight of DMFeFe and DMFeMg sample was 31.1 mg and 22.7 mg, respectively. The heating and cooling rate was 5 K/min. The excess heat capacity associated with the phase transition in DMFeFe was evaluated by subtraction from the data the baseline representing variation in the absence of the phase transitions. The dielectric measurements were performed on pellets made of well-dried samples using a Novocontrol Alpha impedance analyzer (10^{-2}-10^6 Hz). The pellets were located between two copper electrodes of the capacitor with a gap of 0.4 mm. The temperature was controlled by

the Novo-Control Quattro system, with use of a nitrogen gas cryostat. The measurements were taken every 1 deg and temperature stability of the samples was better than 0.1 K. Magnetic properties of a large number of freely oriented single crystals of DMFeMg (about 100 mg in total) were measured using a commercial superconducting quantum interference device (SQUID) magnetometer in the temperature range 2−30 K and in external magnetic fields up to 10 kOe. The background coming from the weakly diamagnetic sample holder (not shown here) was found to be negligible; thus its subtraction was omitted. Also no demagnetization corrections were made to the data reported here. Powder XRD pattern was obtained for all samples on an X'Pert PRO X-ray diffraction system equipped with a PIXcel ultrafast line detector, focusing mirror, and Soller slits for CuKα_1 radiation (λ=1.54056 Å). The single-crystal diffraction data were collected at 298, 190 and 100 K on a KM4-CCD diffractometer operating in κ geometry. Experiments were carried out with Mo *K*α radiation. The low temperature was maintained by open-flow nitrogen gas system (Oxford Cryosystem). Polarized Raman spectra of DMFeFe and DMFeMn single crystals in the 500-3500 cm^{-1} range were measured using a Renishaw InVia Raman spectrometer equipped with confocal DM 2500 Leica optical microscope, a thermoelectrically cooled CCD as a detector and an argon laser operating at 488 nm. Temperature-dependent IR spectra were measured for the samples in KBr pellets in the range of 3800-400 cm^{-1} and in Apiezon N suspension in the range of 500-50 cm^{-1} with the Biorad 575C FT-IR spectrometer using a helium-flow Oxford cryostat. The spectral resolution was 2 cm^{-1}.

Synthesis of the sample

Both compounds were prepared under solvothermal conditions. In order to synthesize DMFeMg, a mixture containing 35 ml of N,N-dimethylformamide (DMF), 25 ml HCOOH, 1.5 mmol $MgCl_2$ and 1.5 mmol $Fe(NO_3)_3$ was heated in a Teflon-lined microwave autoclave at 140^oC for

24 h. Crystals obtained after overnight cooling were washed by ethanol and dried at room temperature. The yield is about 65% based on the $MgCl_2$. The synthesis method of DMFeFe was very similar to the one mentioned above, except of different chemical composition of the mixture that contained 6 mmol $FeCl_2$, 30 ml DMF and 30 ml HCOOH. The yield of obtained black crystals is about 60% based on the $FeCl_2$. The phase purity of both bulk samples was confirmed by a good match of their powder XRD patterns with a simulation from the single-crystal structural data (Figure S1).

Crystallographic Structure Determination

Intensities were measured in ω-scan mode with $\Delta\omega=1.0^{o}$ using CrysAlis CCD program. Absorption was corrected by multi-scan methods, *CrysAlis PRO*, Oxford Diffraction Ltd., Version 1.171.33.42 (release 29-05-2009 CrysAlis171 .NET). An empirical absorption correction was applied using spherical harmonics implemented in SCALE3 ABSPACK scaling algorithm. Due to the disorder of DMA^{+} counterions the nitrogen atoms were refined isotropically. Hydrogen atoms were included in geometric positions (C-H ~0.96 Å) and treated as riding atoms. The $U_{iso}(H)$ values were constrained to be $1.2U_{eq}$(carrier atom). Also the C-N distance restrains were used to obtain reasonable geometry of DMA^{+}. The results of the data collection and refinement along with the crystal description are presented in Table S1.

Results and discussion

Thermal Properties

The DSC measurements of DMFeFe show a sharp heat anomaly at 155.2 K upon warming and 151.8 K upon cooling, characteristic for a first-order phase transition (Figure S2). The change in heat capacity and entropy related to the phase transition is presented in Figure 1. The calculated

change in enthalpy ΔH and entropy ΔS is about 0.33 KJmole^{-1} and 2.44 Jmole^{-1}K^{-1}, respectively. Since according to the X-ray diffraction data the DMA^+ cation occupies three disordered sites at room temperature phase (N=3), a complete ordering of these cations should lead to ΔS = Rln(N) = 9.1 Jmol^{-1}K^{-1}. ΔS is typically smaller than expected if a phase transition has some relaxor character as in $(NH_4)_3Cr(O_2)_4$, $M_{3-x}(NH_4)_xCrO_8$ (M = Na, K, Rb, Cs) and $[(CH_3)_2NH_2][Cd(N_3)_3]$.[17,18] As discussed below, our dielectric studies show relaxor-like dielectric response of DMFeFe. Therefore, the smaller than expected value of ΔS for DMFeFe is consistent with the relaxor character of the phase transition.

Figure S2 shows that DMFeMg does not undergo any phase transitions down to 125 K.

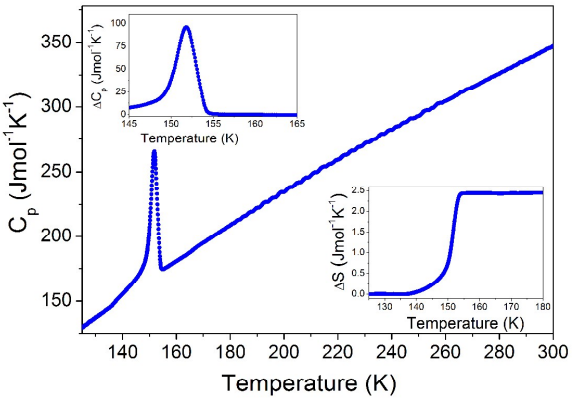

Figure 1. Heat capacity of DMFeFe measured in cooling mode. The insets show the change in C_p and S related to the phase transition.

Dielectric Properties

Figure 2 illustrates temperature dependence of the complex dielectric permittivity $\varepsilon^*(f) = \varepsilon'(f) - i\varepsilon''(f)$ for DMFeFe and DMFeMg samples at various frequencies. The values of the real part of the dielectric permittivity are of the same order for the both materials up to approximately 220 K. Differences in the $\varepsilon'(f)$ may be observed within the high frequency regions where some dc ionic conducting process start to dominate. The characteristic relaxor behavior of the dielectric permittivity can be observed for the investigated samples, in the analyzed temperature range. Moreover, the real component of the permittivity (Figure 2a and 2b) exhibits a step-like increase upon heating. For DMFeFe sample the broad step-like maximum shifts to lower temperatures with decreasing frequency. While reaching the phase transition temperature at the frequency of 50 kHz, the step-like peak stops shifting and seems to be frequency independent (Figure 2a). The observed anomaly can be attributed to the mentioned above phase transition. It should be noted that the dielectric response of niccolite-type DMFeFe is significantly different from that observed for perovskite-type $[(CH_3)_2NH_2][M(HCOO)_3]$ (DMM) with M=Mg, Ni and DMNaFe, for which the step-like peak exhibited strong dependence on probing frequency also in the low-temperature phase.[9,16,19]

At the same time, the bell shape maximum in the imaginary part of dielectric permittivity shifts to lower temperatures with decreasing frequency. Around the phase transition temperature the peak starts to disappear and a new, broad loss peak corresponding to the low-temperature phase appears (Figure 2c). In case of DMFeMg, more significant influence of probing frequency on its dielectric permittivity spectra is observed. However, the dielectric response of this sample does not show any distinct point that could indicate presence of a phase transition. For this material the edge of the step-like real dielectric permittivity shifts to the lower temperature with decreasing frequency (Figure 2b) . The dielectric loss spectra $\varepsilon''(f)$ show the same tendency.

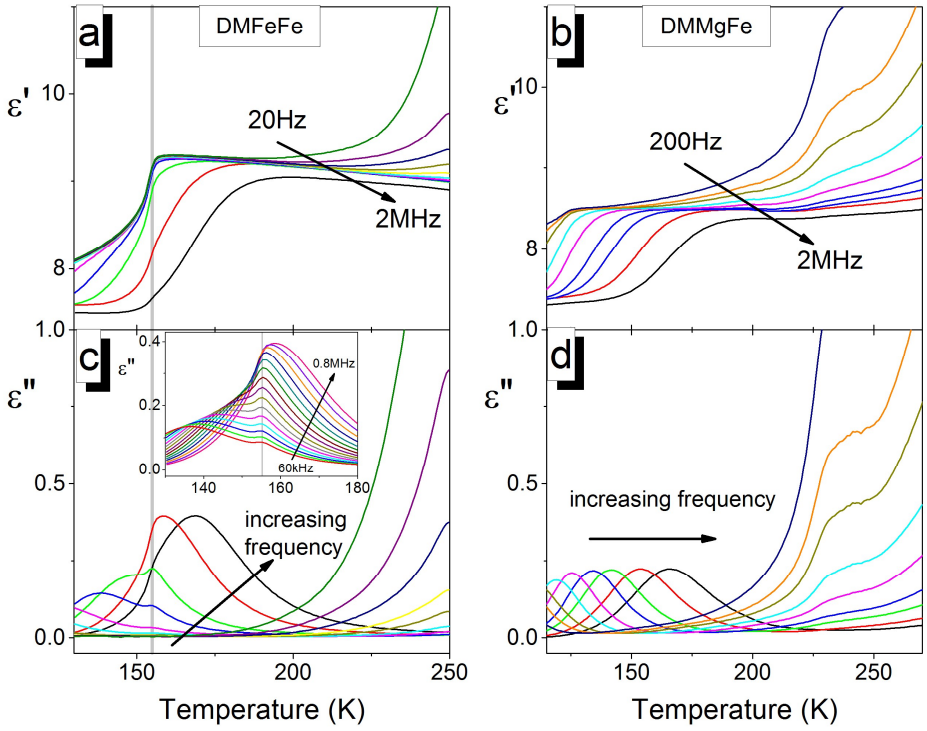

Figure 2. Temperature dependence of the real ε' part of the dielectric permittivity for (a) DMFeFe and (b) DMFeMg. Temperature dependence of the imaginary ε'' part for DMFeFe and DMFeMg are shown in (c) and (d), respectively. Inset on Figure (c) shows imaginary part of dielectric permittivity in the vicinity of the phase transition.

In Figure 3 dielectric response of the studied DMFeFe and DMFeMg samples are presented. It follows from the frequency dependence of the imaginary part of the complex permittivity that for both materials the ε'' exhibits a single relaxation peak characteristic for dipolar relaxation, shifted towards higher frequencies with increasing temperature(c.f. Fig.3a and 3b). Moreover, it is clear from the Cole-Cole plots that the dielectric loss spectra deviate from the classical Debye

behavior for both DMFeFe and DMFeMg samples (c.f. Fig.3c and 3d). The complex plane representation revealed that loss peaks in the analyzed materials seems to be slightly asymmetric at some temperatures and are definitely narrower than a pure Debye peak. The observed non-Debye relaxation behaviour is not surprising at all, as it was found to be characteristic for complex, multicomponent materials. The studied DMFeFe and DMFeMg reveal the anomalous, two-power-law relaxation mechanism represented by low- and high-frequency power-law dependence of the imaginary part of dielectric permittivity on frequency, i.e.:

$$\varepsilon''(f) \propto (f / f_{\max})^{m} \quad \text{for} \quad f < f_{\max},$$
$$\varepsilon''(f) \propto (f / f_{\max})^{n-1} \quad \text{for} \quad f > f_{\max},$$

where $f_{\max}$ denotes the loss peak frequency and the power-law exponents fall in the range of $0 < m, n < 1$.

It is clear from Figure 3a that for DMFeFe strong rise of the dielectric loss spectrum is observed at high frequencies, whereas for DMFeMg significantly weaker changes in the peak amplitude with increasing temperature are observed (see Figure 3b).These results are consistent with the experimental data obtained from the temperature-dependent measurements of the complex permittivity. Additionally, for DMFeFe significant increase in the signal amplitude within the loss peak region is observed upon heating. Moreover, the shape of the peak changes with the increasing temperature. These observations suggest that the effective relaxation response of the sample is governed by contribution of two relaxational processes, one of which is predominant at lower temperatures, and the other one starts to dominate at higher temperatures. The preliminary assumption of two competing relaxational mechanisms may be justified also by the shape of $\varepsilon''(T)$ data (see inset in Figure 2c), however, it requires further, more detailed

studies. For DMFeMg the loss peak shape changes rather slightly as well as the amplitude of the spectra.

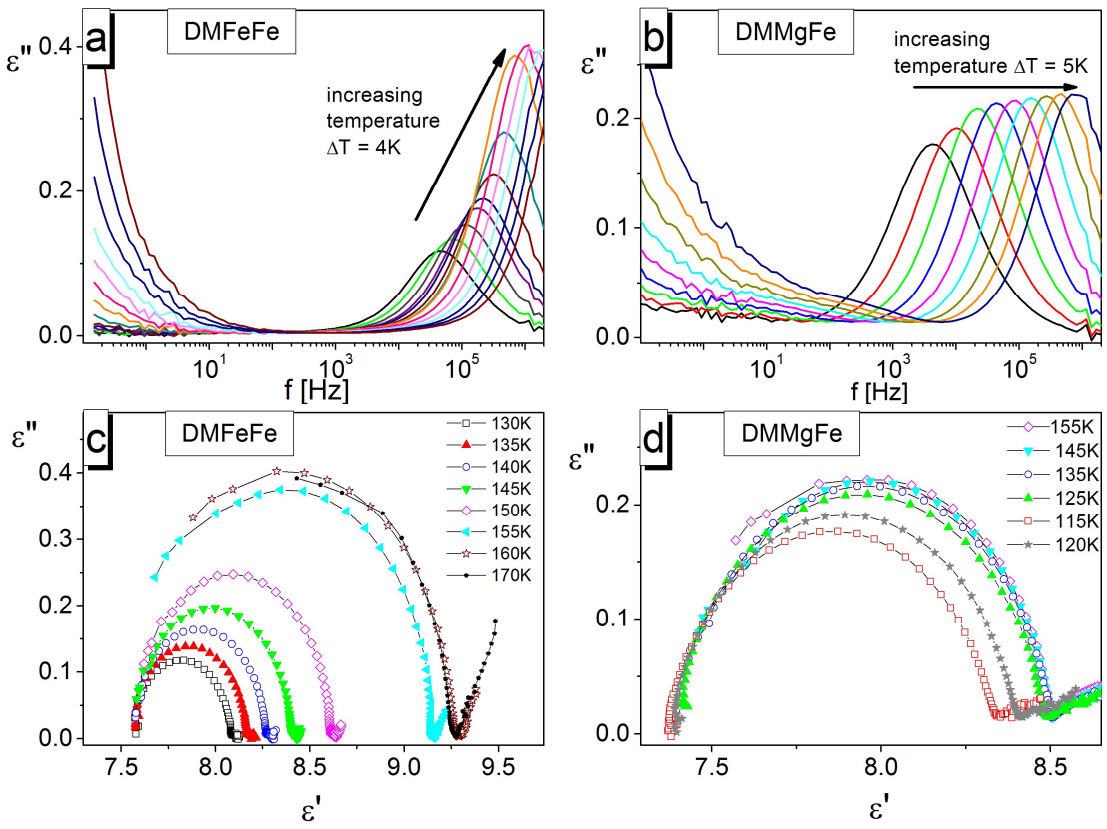

Figure 3. Dielectric spectroscopy data obtained (a)(c) DMFeFe and (b)(d) DMFeMg samples.

Magnetic Properties

Figure 4 displays temperature dependence of the magnetization of DMFeMg measured in an external magnetic field of 100 Oe. As seen, the compound orders magnetically at T_C = 13.5(5) K and the shape of σ(T) measured in the field-cooling regime suggests ferromagnetic character of the ordering. The latter hypothesis is corroborated by a very large difference between the zero-field-cooling and field-cooling curves and by a distinct hysteresis visible in the field dependence

of the magnetization of DMFeMg (see the inset to Figure 4). It is worth noting that the hysteresis can be observed only at relatively low magnetic fields (below about 6 kOe) – at higher fields the compound behaves like a conventional Curie-like paramagnet (not shown here).

Large differences between the FC and ZFC curves (especially the negative magnetization in the ZFC regime, which is of similar magnitude as in the FC regime) and high sensitivity of the magnetic properties of DMFeMg on external magnetic field are characteristic of weak ferromagnetism, which is often observed in metal-organic frameworks.[9,11,20,21] It is commonly known that the origin of the latter phenomena is an antisymmetric exchange or single-ion anisotropy,[22] which are very likely in the compound studied. They often lead to a small canting of the spins in the underlying antiferromagnetic lattice and then result in a small ferromagnetic component of the moments, which is produced perpendicular to the spin-axis of the antiferromagnet. Such a small canting is in general strongly sensitive on temperature, magnetic field and the strength of the coupling between the magnetic ions. Small changes in these parameters may lead to complex magnetic behavior and in some conditions even to reversal of the magnetization sign with decreasing temperature below a certain compensation temperature.[23] The latter effect was however not observed in our sample, therefore further experiments (e.g. neutron diffraction) are needed to reveal the details of the magnetic structure of DMFeMg. It should be noted that the ordering temperature of DMFeMg containing nonmagnetic magnesium ions (13.5(5) K) is much lower than the ordering temperatures of related DMFeFe (37 K), DMFeMn (35 K) and DMFeCo (32 K) compounds with two magnetic sublattices.[15]

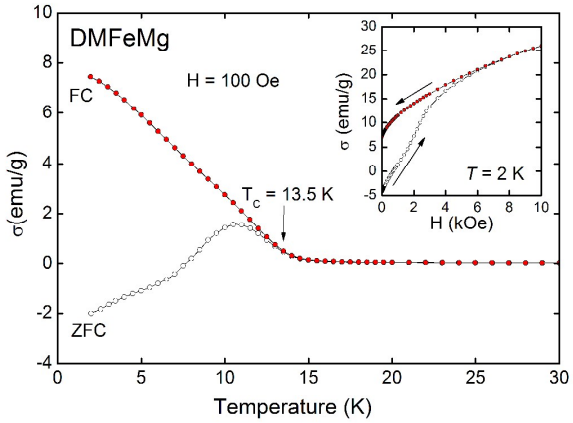

Figure 4. Temperature variation of magnetization σ of DMFeMg measured in zero-field-cooling (ZFC) and field-cooling (FC) regimes; solid lines serve as guides for the eye and the arrow marks the ordering temperature T_C. Inset: field dependence of σ measured at constant temperature upon increasing and decreasing field H (open and closed symbols, respectively); solid lines serve as guides for the eye.

Structural Studies

DMFeMg crystallizes in the trigonal $P\bar{3}1c$ space group. The compound is isomorphic with previously reported DMFeFe, DMFeMn and DMFeCo.[15] The metal centers are bridged by formate ions in the anti-anti mode configuration and form 3D framework that accommodate DMA^+ counterions. Both metal centers possess trigonaly distorted octahedral coordination. Contrary to previously published structures of DMFeM, the metal ions are distributed statistically in DMFeMg over the two available octahedral sites. The Mg1/Fe1 position is occupied by 68% of Mg^{2+} and 32% of Fe^{3+} whereas Mg2/Fe2 site accommodates 32% of Mg^{2+} and 68% of Fe^{3+} (data from the refinement at 100 K). The random distribution of metal ions is reflected in the

length of the M-O distances that at room temperature are equal to 2.0547(13) Å for Mg1/Fe1-O and 2.0202(13) Å for Fe2/Mg2-O bonds (see Table 1). Both distances fall in normal range observed for similar class of materials, *e.g.* the Fe^{3+}-O bond lengths in DMFeM are in the range of 2.007(4)-2.021(2) Å,[15] whereas Mg^{2+}-O bonds in magnesium formates templated by formamidinium and ammonium cations range from 2.0464(11) to 2.0907(11) Å.[6,12]

Similarly to DMM perovskites, DMA^+ counterions are weakly anchored in the voids of $[FeMg(HCOO)_6]_n$ framework. Although the NH_2 groups of DMA^+ are engaged in formation of N–H···O hydrogen bonds with anionic framework, the DMA^+ cations at room temperature are significantly disordered over six various positions that are illustrated in Figure 5. All of them have the same hydrogen bond geometry that is listed in Table 2. Thermal ellipsoids of carbon atoms from DMA^+ are in all measured temperatures elongated in *c* direction that indicates easy movements of counterions along trigonal 3-fold axis that have not been observed in DMM formates. With temperature lowering, down to 100 K, the interatomic distances change insignificantly and are almost equal within 3σ limit (where σ is a standard deviation) to the room-temperature distances, see Table 1. The number of disordered DMA^+ orientations does not change so does the geometry of hydrogen bonding. The crystal structure is stable and do not experience any structural phase transition.

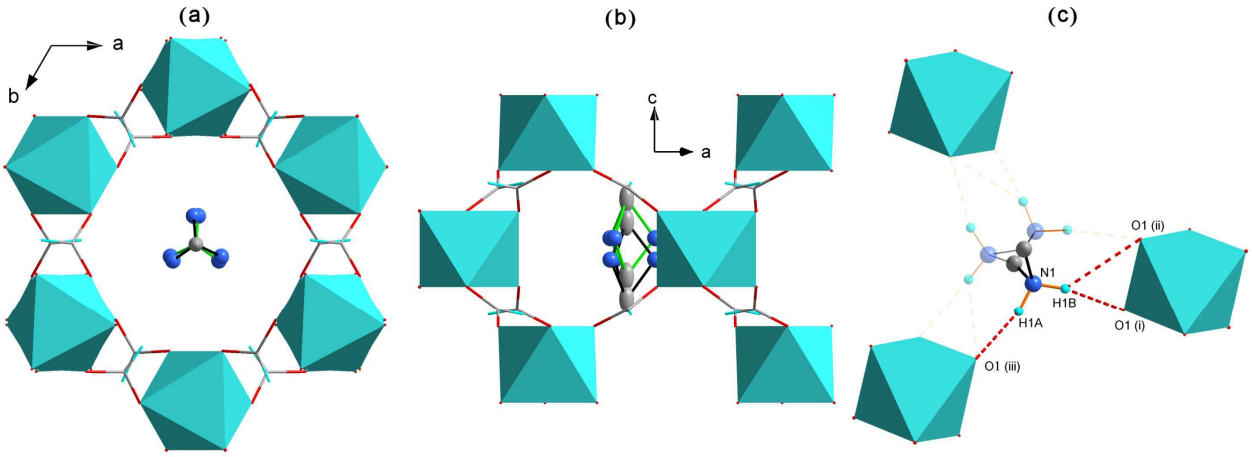

Figure 5. The view of the structure cavities with DMA^+ ions along (a) *c* direction and (b) *b* direction. DMA^+ is disordered over six equally probable positions. The hydrogen atoms have been omitted for the picture clarity. (c) N-H···O hydrogen bonds between DMA^+ ions and rigid $FeMg(HCOO)_6^-$ groups for three different settings of DMA^+.

Table 1. Selected geometric parameters (Å) in DMAFeMg.

(100 K)			
Fe1/Mg1—O1 x 6	2.0547 (13)	O1—C1	1.243 (2)
Fe2/Mg2—O2 x 6	2.0202 (13)	O2—C1	1.257 (2)
(190 K)			
Fe1/Mg1—O1	2.0568 (12)	O1—C1	1.239 (2)
Fe2/Mg2—O2	2.0209 (12)	O2—C1	1.252 (2)
(298K)			
Fe1/Mg1—O1	2.0566 (12)	O1—C1	1.229 (2)
Fe2/Mg2—O2	2.0193 (12)	O2—C1	1.245 (2)

Table 2. The geometries of the N-H···O hydrogen bonds between the DMA^+ cations and the anionic framework (distances, Å; angles, °).

D—H···*A*	*D*—H (Å)	H···*A* (Å)	*D*···*A* (Å)	*D*—H···*A* (°)
(100 K)				
N1—H1B···O1^{i}	0.89	2.41	3.161 (15)	142.6
N1—H1B···O1^{ii}	0.89	2.54	3.248 (18)	136.8
N1—H1A···O1^{iii}	0.89	2.18	3.007 (17)	155.4
(190 K)				
N1—H1A···O1^{i}	0.89	2.43	3.175 (15)	140.9
N1—H1A···O1^{ii}	0.89	2.48	3.211 (17)	140.0
N1—H1B···O1^{iii}	0.89	2.20	3.029 (17)	155.0
(298 K)				
N1—H1A···O1^{i}	0.91	2.43	3.202 (14)	142.2
N1—H1A···O1^{ii}	0.91	2.48	3.195 (17)	135.7
N1—H1B···O1^{iii}	0.95	2.18	3.058 (17)	152.7

Symmetry code(s): (i) *x*-*y*+1, -*y*+1, *z*+1/2; (ii) *y*, -*x*+*y*, -*z*+1; (iii) -*x*, -*y*+1, -*z*+1.

Vibrational Studies – Assignment of Modes

The correlation diagram showing number of expected internal modes of formate and DMA^+ ions as well as lattice modes for the $P\bar{3}1c$ and $R\bar{3}c$ structures is presented in Table S2. Since the DMA^+ cations are disordered at room temperature, the calculated number of modes for this cation are presented only for the low-temperature ordered phase. This table shows that the number of vibrational modes of the $P\bar{3}1c$ niccolite structure should be doubled when compared to the room-temperature $R\bar{3}c$ structure of DMM perovskites, where M=Mn, Ni, Mg, Zn, Co.[9]

The polarized Raman and polycrystalline IR spectra of DMFeFe and DMFeMg are presented in Figures 6 and S3-S8, Supporting Information. The observed IR and Raman frequencies (in cm^{-1}) are collected in Tables S3 and S4 together with the proposed assignments. The obtained results

show that vibrational modes of the methyl and CNC groups of the DMA^+ cation are observed at very similar frequencies to those found for DMM formates.[8,9] However, $\nu(NH_2)$ and $\rho(NH_2)$ modes are observed at higher and lower frequencies, respectively.[8,9] This result indicates significantly weaker H-bond strength in the niccolite-type framework when compared to the perovskite-type framework. Significant differences can also be noted in frequencies of formate groups. This behavior reflects different symmetry of these groups in the niccolite and perovskite framework. In particular, the $HCOO^-$ ions in DMM formates with perovskite structure are symmetric with two equal C-O bond lengths,[9] but asymmetric in the niccolite framework (see Table 1). Our results also show that the room-temperature spectra of DMFeFe are very similar to the spectra of DMFeMg. However, it can be noticed that the $\nu_4(HCOO^-)$ mode shift towards higher frequency by 15 cm^{-1} when Fe(II) is replaced by Mg(II). Similar behavior was observed previously by us for $[NH_4][M(HCOO)_3]$ formates.[6] This behavior indicates stronger C-O bonds in the magnesium compounds due to the fact that Mg-O bond is more labile than M-O bond with M=Fe, Co, Zn, Ni since Mg is a softer Lewis acid than the mentioned above divalent cations.[24]

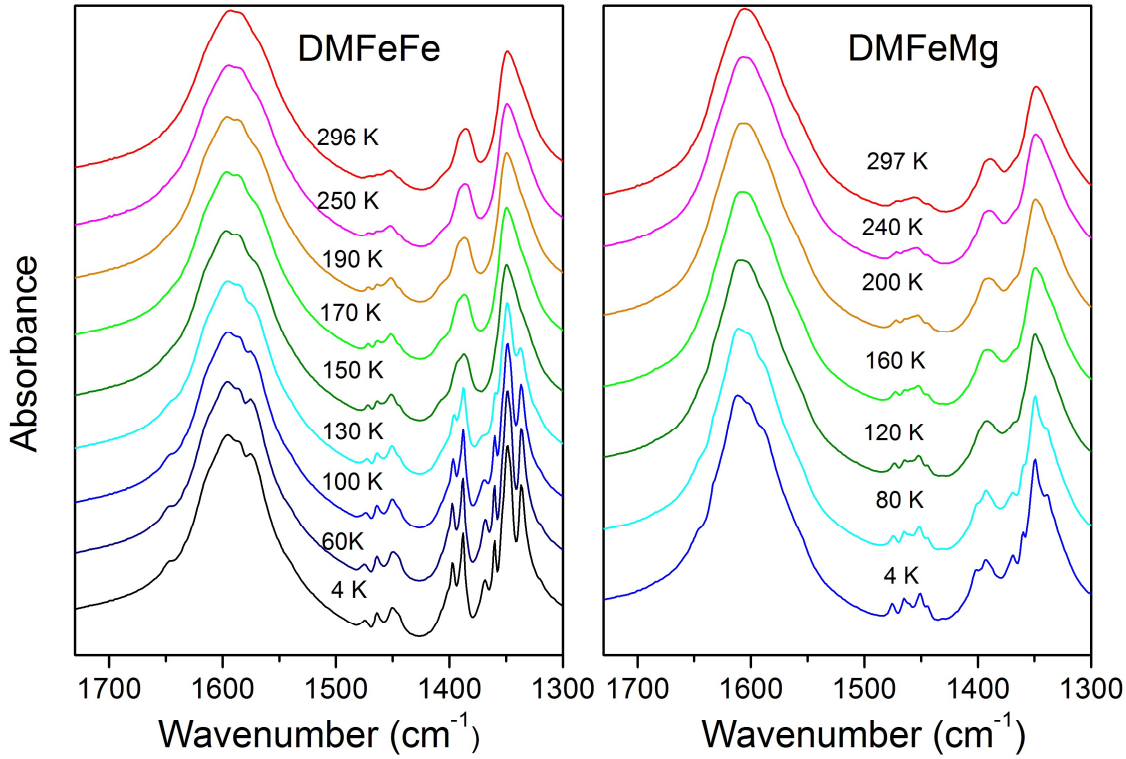

Figure 6. Detail of the IR spectra results corresponding to the spectral range 1300-1730 cm^{-1} for (a) DMFeFe and (b) DMFeMg.

Temperature-dependent Raman and IR Studies

Temperature-dependent IR studies show that lowering of temperature leads to narrowing and shifts of bands. As a result, many not resolved and weak bands overlapped by stronger ones become clearly visible at 4 K temperature (see Figs. S5-S8). It should be noticed that narrowing of bands is much more pronounced for DMFeFe than DMFeMg (see for instance Figures 6, S7 and S8). This behavior is consistent with ordering of the DMA^+ cations in DMFeFe at low temperatures and disorder of these cations in DMFeMg down to 4 K.

Figures 7, S9 and S10 show temperature evolution of a few selected vibrational frequencies and FWHMs for different molecular subunits of the studied compounds. These figures show very clear discontinuous changes in frequency or changes in the slope of frequencies vs temperature at the structural phase transition found in the DSC measurements of DMFeFe at 151.8 K upon cooling. This behavior is consistent with the first-order character of this transition. As can be seen, clear changes are observed both for the DMA^+ and formate modes, and this behavior indicates that the phase transition is related to distortion of both organic cation and iron-formate framework. Figures 7, S9 and S10 also show that upon cooling DMFeFe the FWHM values of the analyzed bands exhibit weak decrease down to about 150 K followed by much faster decrease below 150 K. Especially pronounced changes are observed for the $\rho(NH_2)$ and lattice modes (see Figures 7 and S10). This behavior confirms that the phase transition in DMFeFe niccolite is associated with ordering of DMA^+ cations, similarly as in DMM perovskites with M=Mg, Zn, Mn, Ni, Co, Fe. However, closer inspection of the IR data for DMFeFe and DMM compounds show significant differences. Firstly, the ν_{as}(CNC) mode of DMMn and DMNi exhibited very pronounced shift at the phase transition towards higher frequencies (by about 3 cm^{-1}),[9] whereas the corresponding mode of DMFeFe shows change in the slope of frequency vs temperature only. This result indicates that changes in the C-N bond lengths at T_c are much more pronounced for the DMMn and DMNi perovskites than DMFeFe niccolite. Secondly, the $\rho(NH_2)$ mode exhibited upon cooling shift to higher frequency at T_c for DMMn and DMNi and this result is consistent with increased strength of hydrogen bonds in the low-temperature structure of the perovskites.[9] In case of DMFeFe niccolite the corresponding mode shifts to lower frequency at T_c indicating a slight decrease of the hydrogen bond strengths at T_c. Thirdly, FWHM of the $\rho(NH_2)$ band exhibited more pronounced decrease upon cooling for the perovskites (FWHM decreased nearly

5 times when temperature changed from room temperature to 4 K[9]) than DMFeFe niccolite (FWHM decreased twice). This result points to more significant contribution of the DMA^+ dynamics to the phase transition mechanism in perovskites when compared to DMFeFe niccolite.

In contrast to clear changes at T_c observed for DMFeFe, the temperature dependence of IR frequencies and FWHM values of DMFeMg do not show any anomalies upon cooling. This result proves that this compound does not exhibit any structural phase transition. It is worth noting that whereas FWHM of the $\rho(NH_2)$ bands decreases strongly for DMFeFe (from about 14 cm^{-1} at room temperature to less than 7 cm^{-1} at 4 K), the temperature dependence of FWHM for this modes is weak for DMFeMg (the FWHM changes from about 13 cm^{-1} at 297 K to 11 cm^{-1} at 4 K). This behavior proves that the DMA^+ cations are disordered at low temperatures, i.e. the dynamical disorder at room temperature evolves into static disorder at low temperatures and this process is not associated with any structural deformation.

IR spectra of DMFeFe show also some changes in frequencies and FWHM values near about 35 K (see Figs. 7, S9 and S10). This temperature corresponds well to the 37 K temperature where long-range magnetic order appears.[14] It seems therefore reasonable to assume these changes to spin-phonon coupling. Such coupling is expected to shift frequency of a vibrational mode by:

$$\Delta\omega_i \equiv \lambda\langle S_i S_j \rangle \qquad (2)$$

where the spin-phonon coupling constant λ is different for different phonons and can have either a positive or a negative sign.[25] Significant changes should be observed for phonons, which involve motions that modulate spin exchange coupling. In the metal-formate framework compounds the indirect magnetic exchange is expected to occur through the formate ligands, and therefore weak anomalies are expected for modes of the metal-formate framework. Our previous

studies of DMMn and DMNi were consistent with this assumption since they revealed no anomalies for DMA^+ modes and very weak anomalies for the $\nu_3(HCOO^-)$ modes, i.e. these modes showed downward frequency shifts at the magnetic transitions by less than 0.2 cm^{-1}.[9] Our present data for DMFeFe show more pronounced shifts, up to 0.6 cm^{-1}. More interestingly, these anomalies are observed also for the DMA^+ modes. Origin of this behavior is not clear but we cannot exclude that the magnetic phase transition at 37 K is associated also with some subtle change of the crystal structure.

The obtained data give evidence that the structural phase transition in DMFeFe is associated with ordering of DMA^+ cations. Thus there are no doubts that cooperative freezing of the reorientational motions of DMA^+ cations plays important role in the phase transition mechanism. The question that arises is why DMFeMg does not exhibit any structural transition in spite of very similar structure and freezing of the orientational motions of DMA^+ at low temperatures. No phase transition was also reported for DMFeMn and DMFeCo compounds.[15] This difference is especially striking since order-disorder transitions were found in all DMM perovskites with M=Mg, Zn, Mn, Co, Fe and Ni.[5,8,9] Moreover, substitution of Mg for other metal ions resulted in pronounced increase of the phase transition temperature,[19] but this behavior is not observed for DMFeMg niccolite. First of all, it is worth noting that studies of phase transitions in metal formate frameworks indicated that a key role in these transitions are played by the organic cations rather than the host frameworks.[5,8,9] However, for a more flexible framework containing N_3^- linkers, like in $[(CH_3)_2NH_2][Cd(N_3)_3]$ perovskite, the driving force for the structural phase transition was found to be mainly deformation of the framework, although this deformation is also associated with ordering of DMA^+ cations.[18] Thus the lack of phase transition in DMFeM niccolites (M=Mg, Mn, Co) and presence of order-disorder transitions in DMM perovskites as well as $[CH_3NH_2(CH_2)_2NH_2CH_3][Zn(HCOO)_6]$ and $[NH_3(CH_2)_4NH_3][Mg(HCOO)_6]$ niccolites

with divalent metal cations[5,6,8,9,26] can be attributed to less flexible and deformable framework in the former case due to presence of trivalent iron ions. This explanation is, however, not valid for DMFeFe. Since the unique feature of DMFeFe is presence of intervalence charge-transfer (IVCT) transition, which indicates presence of electron transfer from divalent to trivalent iron ions (DMFeFe is type II valence-trapped compound[13]), we suppose that different structural stability of DMFeFe, when compared to DMFeMg, DMFeMn and DMFeCo, may be related to its electronic properties and change of the rate of electron transfer with decreasing temperature.

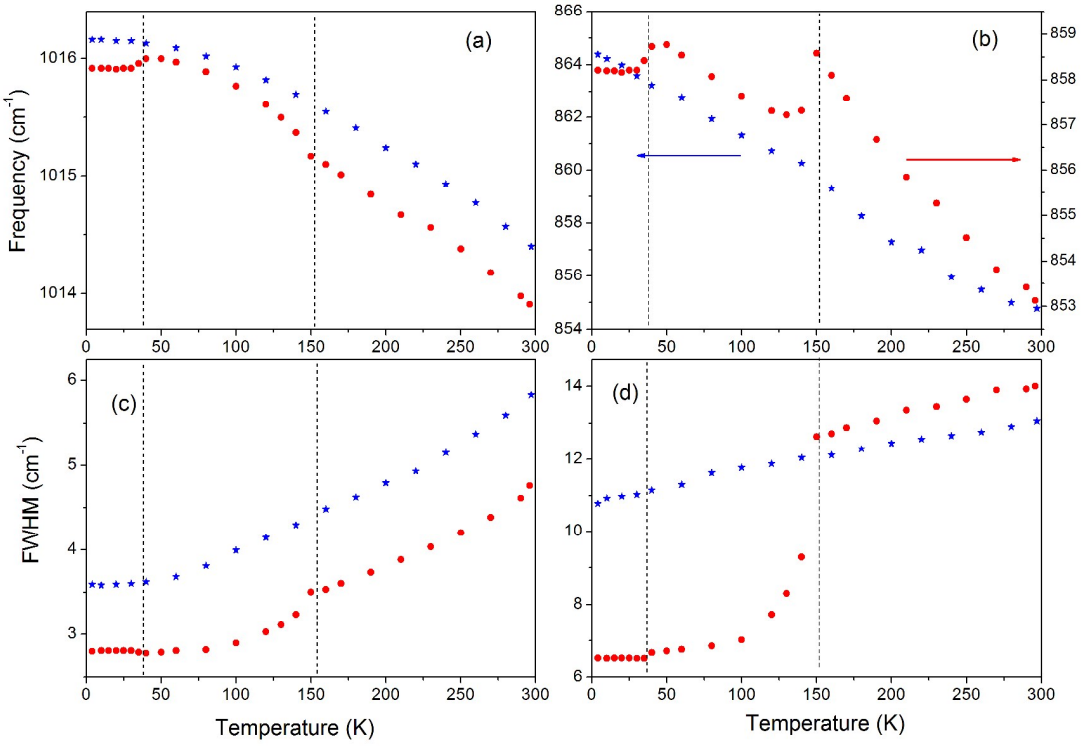

Figure 7. Temperature dependence of frequency for the IR-active (a) ν_{as}(CNC) and (b) $\rho(NH_2)$ modes as well as FWHM of the IR-active (c) ν_{as}(CNC) and (d) $\rho(NH_2)$ modes. Red circles correspond to DMFeFe and blue stars to DMFeMg. The vertical lines indicate the temperatures where DMFeFe undergoes the structural phase transition are to guide the eye.

Conclusions

We have synthesized novel niccolite-type metal formate framework compound DMFeMg and already reported DMFeFe. These compounds have been characterized by DSC and temperature-dependent X-ray diffraction, dielectric and vibrational spectroscopy methods. The obtained data show that contrary to the known DMFeFe, DMFeMn and DMFeCo compounds, the metal ions in DMFeMg are distributed statistically over the two available octahedral sites. Furthermore, DMA^+ cations remain disordered in DMFeMg even at low temperatures, i.e. these cations rotate dynamically at room temperature but this reorientational motion slows down upon cooling and freezes at low temperatures leading to static disorder at low temperatures. Thus DMFeMg does not exhibit any low-temperature structural phase transition. This behavior is very different from DMFeFe for which freezing of dynamical disorder led to structural phase transitions into antiferroelectric phase with ordered DMA^+ cations. We suppose that this difference can be related to additional electronic contribution to the phase transition mechanism in DMFeFe.

Our results also show that the dielectric response of niccolite DMFeFe is significantly different from that observed for the perovskite-type DMM and DMNaFe compounds, that is, the step-like peak in $\varepsilon'(f)$ seems to be frequency independent in the low-temperature phase of DMFeFe but it exhibited strong dependence on probing frequency in the low-temperature phase of the perovskites.[9,16,19] Spectroscopic data provide further evidence for significantly different character of the phase transitions in DMFeFe niccolite and DMM perovskites. Namely, they reveal less pronounced role of DMA^+ dynamics in the phase transition mechanism in DMFeFe compared to the DMM perovskites.

Acknowledgements

This research was supported by the National Center for Science (NCN) in Poland under project No. DEC-2013/11/B/ST5/01058.

Notes

[a]Institute of Low Temperature and Structure Research, Polish Academy of Sciences, Box 1410, 50-950 Wrocław 2, Poland; m.maczka@int.pan.wroc.pl; phone: +48-713954161; fax: +48-713441029

[b]Faculty of Fundamental Problems of Technology, Wrocław University of Technology, Wybrzeże Wyspiańskiego 27, 50-370
Wrocław, Poland

Electronic Supplementary Information (ESI) available: X-ray crystallographic information files (CIF) for crystal structures of DMFeFe at 298, 190 and 100 K. Figures S1-S10: Powder X-ray diffraction, DSC traces, IR and Raman spectra, temperature dependence of bandwidths and frequencies. Tables S1-S4: X-ray data collection and refinement parameters, the correlation diagram showing the correspondence between the optical modes in the $P\bar{3}1c$ and $R\bar{3}c$ structures, and Raman and IR frequencies for all samples at 297 and 4 K.

References

1 *(a)* J. Y. Lee, O. K. Farha, J. Roberts, K. A. Scheidt, S. B. T. Nguyen, J. T. Hupp, *Chem. Soc. Rev.*, 2009, **38**, 1450; *(b)* L. E. Kreno, K. Leong, O. K. Farha, M. Allendorf, R. P. V. Duyne, J. T.

Hupp, *Chem. Rev.*, 2012, **112**, 1105; *(c)* Y. Cui, Y. Yue, G. Qian, B. Chen, *Chem. Rev.*, 2012, **112**, 1126.

2 R. Shang, S. Chen, Z. M. Wang, S. Gao, in *Metal-Organic Framework Materials*. Edited by R. L. MacGillivray and C. M. Lukehart., John Wiley & Sons Ltd., 2014, pp. 221-238.

3 M. Guo, H. L. Cai, R. G. Xiong, *Inorg. Chem. Commun*., 2010, **13**, 1590.

4 W. Zhang and R. G. Xiong, *Chem. Rev*., 2012, **112**, 1163.

5 *(a)* P. Jain, V. Ramachandran, R. J. Clark, H. D. Zhou, B. H. Toby, N. S. Dalal, H. W. Kroto, A. K. J. Cheetham, *J. Am. Chem. Soc*., 2009, **131**, 13625; *(b)* D. W. Fu, W. Zhang, H. L. Cai, Y. Zhang, J. Z. Ge, R. G. Xiong, S. D. Huang, T. Nakamura, *Angew. Chem. Int. Ed*., 2011, **50**, 11947.

6 *(a)* G. C. Xu, W. Zhang, X. M. Ma, Y. H. Hen, L. Zhang, H. L. Cai, Z. M. Wang, R. G. Xiong, S. J. Gao, *J. Am. Chem. Soc*., 2011, **133**, 14948; *(b)* M. Mączka, A. Pietraszko, B. Macalik, K. Hermanowicz, *Inorg. Chem*., 2014, **53**, 787; *(c)* R. Shang, G. C. Xu, Z. M. Wang, S. Gao, *Chem. Eur. J*., 2014, **20**, 1146.

7 *(a)* D. Di Sante, A. Stroppa, P. Jain, S. Picozzi, *J. Am. Chem. Soc*., 2013, **135**, 18126; *(b)* W. Wang, L.-Q. Yan, J.-Z. Cong, Y.-L. Zhao, F. Wang, S.-P. Shen, T. Zhou, D. Zhang, S.-G. Wang, X.-F. Han, Y. Sun, *Sci. Rep*., 2013, **3**, 2024.

8 *(a)* M. Sánchez-Andújar, L.C. Gómez-Aguirre, B. Pato Dolán, S. Yáñez-Vilar, R. Artiga, A. L. Llamas-Saiz, R. S. Manna, S. Schnelle, M. Lang, F. Ritter, A. A. Haghighirad, M. A. Señaris-Rodriguez, *CrystEngComm*., 2014, **16**, 3558ł *(b)* M. Mączka, M. Ptak, L. Macalik, *Vib. Spectrosc*., 2014, **71**, 98; *(c)* M. Mączka, W. Zierkiewicz, D. Michalska, J. Hanuza, *Spectrochim. Acta A*., 2014, **128**, 6740.

9 M. Mączka, A. Gągor, B. Macalik, A. Pikul, M. Ptak, J. Hanuza, *Inorg. Chem*., 2014, **53**, 457.

10 *(a)* Y. Tian, W. Wang, Y. Chai, J. Cong, S. Shen, L. Yan, S. Wang, X. Han, Y. Sun, *Phys. Rev. Lett*., 2014, **112**, 017202; *(b)* M. Mączka, P. Kadłubański, P. T. C. Freire, B. Macalik, W. Paraguassu, K. Hermanowicz, J. Hanuza, *Inorg. Chem*., 2014, **53**, 9615; *(c)* M. Mączka, M. Ptak, S. Kojima, *Appl. Phys. Lett*., 2014, **104**, 222903.

11 M. Mączka, A. Ciupa, A. Gągor, A. Sieradzki, A. Pikul, B. Macalik, M. Drozd, *Inorg. Chem*., 2014, **53**, 5260.

12 *(a)* A. Rossin, M. R. Chierotti, G. Giambiastiani, R. Gobetto, M. Peruzzini, *Cryst. Eng. Comm*., 2012, **14**, 4454; *(b)* T. Besara, P. Jain, N. S. Dalal, P. L. Kuhns, A. P. Reyes, H. W. Kroto, A. K. Cheetham, *J. Proc. Nat. Acad. Soc*., 2011, **108**, 6828.

13 K. S. Hagen, S. G. Naik, B. H. Huynh, A. Masello, G. Christou, *J. Am. Chem. Soc*., 2009, **131**, 7516.

14 L. Cañadillas-Delgado, O. Fabelo, J. A. Rodríguez-Velamazán, M.-H. Lemėe-Cailleau, S. A. Mason, E. Pardo, F. Lloret, J.-P. Zhao, X.-H. Bu, V. Simonet, C. V. Colin, J. Rodríguez-Carvajal, *J. Am. Chem. Soc*., 2012, **134**, 19772.

15 J.-P. Zhao, B.-W. Hu, F. Lloret, J. Tao, Q. Yang, X.-F. Zhang, X.-H. Bu, *Inorg. Chem*., 2010, **49**, 10390.

16 M. Mączka, A. Pietraszko, L. Macalik, A. Sieradzki, J. Trzmiel, A.Pikul, *Dalton Trans*., 2014, **43**, 17075.

17 *(a)* R. Samantaray, R. J. Clark, E. S. Choi, H. Zhou, N. S. Dalal, *J. Am. Chem. Soc*., 2011, **133**, 3792; *(b)* R. Samantaray, R. J. Clark, E. S. Choi, N. S. Dalal, *J. Am. Chem. Soc*., 2012, **134**, 15953.

18 Y. Z. Du, T. T. Xu, B. Huang, Y. J. Su, W. Xue, C. T. He, W. X. Zhang, X. M. Chen, *Angew. Chem. Int. Ed*., 2015, **54**, 914.

19 B. Pato Dolán, M. Sánchez-Andújar, L. C. Gómez-Aguirre, S. Yáñez-Vilar, J. Lopez-Beceiro, C. Gracia-Fernandez, A. A. Haghighirad, F. Ritter, S. Castro-Garcia, M. A. Señaris-Rodriguez, *Phys. Chem. Chem. Phys*., 2012, **14**, 8498.

20 *(a)* X. Y. Wang, L. Gan, S. W. Zhang, S. Gao, *Inorg. Chem*., 2004, **43**, 4615; *(b)* Z. Wang, B. Zhang, K. Inoue, H. Fujiwara, T. Otsuka, H. Kobayashi, M. Kurmoo, *Inorg. Chem*., 2007, **46**, 437.

21 A. Ciupa, M. Mączka, A. Gągor, A. Pikul, E. Kucharska, J. Hanuza, A. Sieradzki, *Polyhedron*, 2015, **85**, 137.

22 *(a)* I. Dzyaloshinsky, *J. Phys. Chem. Solids*, 1958, **4**, 241; *(b)* T. Moriya, *Phys. Rev*., 1960, **120**, 91.

23 N. Dasari, P. Mandal, A. Sundaresan, N. S. Vidhyadhiraja, *Europhys. Lett*., 2012, **99**, 17008.

24 T. F. Liu, L. Zou, D. Feng, Y. P. Chen, S. Fordham, X. Wang, Y. Liu, H. C. Zhou, *J. Am. Chem. Soc*., 2014, **136**, 7813.

25 *(a)* J. I. Lee, T. W. Noh, J. S. Bae, I. S. Yang, T. Takeda, R. Kanno, *Phys. Rev. B*, 2004, **69**, 214428; *(b)* M. Ptak, M. Maczka, K. Hermanowicz, A. Pikul, J. Hanuza, *J. Solid State Chem*., 2013, **199**, 295.

26 M.-Y. Li, M. Kurmoo, Z.-M. Wang, S. Gao, *Chem. Asian J*., 2011, **6**, 3084.

We report temperature-dependent studies of $[(CH_3)_2NH_2]Fe^{III}Mg^{II}(HCOO)_6]$ and $[(CH_3)_2NH_2]Fe^{III}Fe^{II}(HCOO)_6]$ and discuss origin of different behavior of the both compounds.